Geoengineering via solar radiation management as a feedback control problem: Controller design for disturbance rejection

Steven R. Weller and Brenton P. Schulz

Abstract— **Recent research has proposed the use of feedback of the observed climate to adjust the radiative forcing of solar radiation management (SRM)-based geoengineering schemes, which involve deliberate and large-scale intervention in the planetary environment to counteract anthropogenic climate change. Feedback in an SRM scheme has the potential to compensate for uncertainty in both the forcing and the climate response, and for unexpected changes in the climate system. The long-term warming effects arising from anthropogenic emission of greenhouse gases are thereby (at least partially) offset, in such a way that neither natural climate variability nor measurement noise is unduly amplified. In this paper SRM is framed as a feedback control problem for disturbance rejection, drawing on H_∞-synthesis as a formal framework in which the effect of anthropogenic climate disturbances can be minimized. The effectiveness of both an H_∞-suboptimal SRM controller and a simple proportional-integral (PI) controller is demonstrated on the reduced-complexity climate model MAGICC. The extent and speed with which negative radiative forcing could feasibly be implemented and sustained impose tight constraints on the effectiveness of the control actuation authority in an SRM climate control loop. This in turn suggests caution in relying heavily on feedback to counterbalance uncertainty in the climate system when implementing SRM.**

I. INTRODUCTION

The limited effectiveness of the emissions mitigation-based response to the risks posed by anthropogenic climate change has prompted a network of scientists, entrepreneurs and advocates to consider a "Plan B" response known as *geoengineering*. Also known as climate engineering, geo-engineering involves deliberate and large-scale interventions in the Earths climatic system to counter impacts of climate change such as sea level rise, more severe weather extremes, and ocean acidification [1], [2].

One broad class of geoengineering responses known as *solar radiation management (SRM)* proposes to create a cooling effect by reflecting a fraction of the incident solar radiation before it can cause warming using, for example, injection of sulphate aerosols into the stratosphere [3] or marine cloud brightening [4]. In the event that SRM was ever employed, measurements of the observed climate would almost inevitably be used to inform the determination of the negative radiative forcing needed to offset some fraction of the radiative forcing due to anthropogenic emission of greenhouse gases (GHGs). This would in effect establish a closed-loop system with the global climate as the plant, and with the influence of a policy-based geoengineering response modeled as a feedback controller [5].

This paper examines key control-theoretic implications of framing SRM as a feedback control design problem. The feedback controller structure proposed in this paper controls the amount of SRM forcing needed to (at least partially) offset the rise in global-mean surface temperature due to anthropogenic forcing, subject to natural variability in radiative forcing.

Several authors have recently proposed the use of feedback of the observed climate to adjust the radiative forcing in SRM-based approaches to geoengineering [6] [5], [7], [8]. The use of feedback, it is argued, would compensate for uncertainty in both the forcing and the climate response, and for unexpected changes in the climate system.

Using a simple box-diffusion climate model, MacMartin et al. [5] design a proportional-integral (PI) control law for SRM. An unsettling conclusion of the approach in [5] is that the well-known waterbed effect induces amplification of natural climate variability for time delays as short as 1–2 years. This is principally due to measurements of global-mean surface temperatures in [5] being averaged over several years, thereby introducing a phase shift in the open-loop system similar to that of a pure time delay, with deleterious consequences for stability margins and peak sensitivity to disturbances.

In this paper, we take a different approach, instead framing SRM controller design as an optimal disturbance rejection problem in which the worst-case impact of climatic disturbances is minimized, whilst also steering the global-mean temperature to a desired setpoint. This leads naturally to consideration of H_∞-synthesis as a formal framework for SRM controller design, but we also demonstrate that a simple PI controller is able to achieve similar performance on the climate model MAGICC (Model for the Assessment of Greenhouse-gas Induced Climate Change). The extent and speed with which solar radiation management could likely be implemented pose tight constraints on the effectiveness of the control actuation authority in an SRM control loop, thereby placing limits on the ability for feedback to compensate for the presence of climatic uncertainty.

The paper is organized as follows. In §II we present the problem setup and the control objectives. In §III the H_∞-synthesis approach to control design is reviewed. Simulation results with both a simple linear climate model and a more complex real-world proxy model are presented in §IV. Conclusions are drawn in §V.

Steven R. Weller and Brenton P. Schulz are with the School of Electrical Engineering and Computer Science, University of Newcastle, Callaghan, NSW 2308, Australia. steven.weller@newcastle.edu.au, brenton.schulz@uon.edu.au

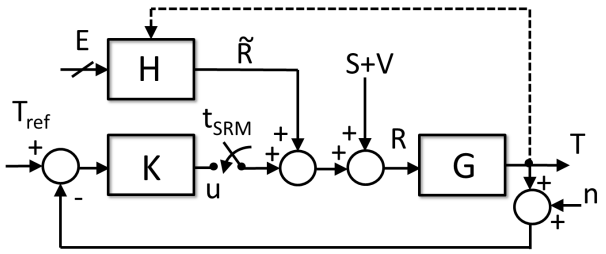

Fig. 1. Block diagram of the solar radiation management (SRM) control problem. Climate model G with output temperature anomaly T is driven by net radiative forcing R comprised of anthropogenic radiative forcing $\widetilde{R}$ from GHG emissions E, volcanic forcing V, solar forcing S and the influence of the SRM controller K for time $t \geq t_{\mathrm{SRM}}$. The dashed line depicts the influence of climate feedbacks on the gas-cycle model H.

II. PROBLEM SETUP AND CONTROL OBJECTIVES

A. System setup

A block diagram of the solar radiation management control problem is shown in Fig. 1. The output of the climate system G is the global-mean surface temperature anomaly T (°C) defined relative to the temperature at the commencement of the industrial era, here taken as the year 1765. The input to G is the net radiative forcing (RF) applied to the climate system at the tropopause, denoted R (Wm^{-2}), also defined as an anomaly relative to pre-industrial forcing.

System H in Fig. 1 is a gas-cycle model which takes as input the annual global anthropogenic emissions E of CO_2 and other greenhouse gases (GHGs) arising from fossil fuel emissions and other industrial sources, together with land-use changes, emissions of aerosols and tropospheric ozone precursors [9]. The influence of emissions E on the climate system is modeled via an additive net anthropogenic radiative forcing term, denoted $\widetilde{R}$.

At time t_{SRM} the solar radiation management (SRM) scheme is initiated by switching controller K into the system, thereby generating an additional (negative) radiative forcing u in order to drive temperature T towards the setpoint temperature T_{ref}.

The dashed line in Fig. 1 represents the various influences of temperature on the global carbon cycle, known as climate feedbacks, e.g. the temperature-dependence of the rate of atmospheric carbon uptake by the terrestrial biosphere.

B. Climate models

Following [7], we distinguish between the *design* model and the *real-world proxy* model. The design model is used for the purposes of controller design, while the resulting controller is tested with the real-world proxy model.

A range of numerical climate models are available for use as real-world proxies for the purposes of simulating the dynamic response of the global climate to solar radiation management. Comprehensive atmosphere–ocean general circulation models (AOGCMs), for example, simulate the combined thermal response of the atmosphere, ocean, land surface and cryosphere to net radiative forcing. The high spatio-temporal resolution of AOGCMs makes them computationally intensive, however, thereby limiting their applicability in contexts requiring repeated simulation runs.

The real-world proxy model employed in this paper is MAGICC (Model for the Assessment of Greenhouse-gas Induced Climate Change), version 6. MAGICC is a freely available reduced-complexity model which has been used in several Intergovernmental Panel on Climate Change (IPCC) assessment reports to produce projections of future global mean temperature.

MAGICC is a so-called simple climate model capable of simulating several hundred years of climatic response to a given emissions scenario in a fraction of a second on a desktop computer. Nevertheless, the dynamics of MAGICC are nonlinear, high-order ($n \approx 100$) and time-varying [9], making MAGICC poorly suited to the application of control design methodologies requiring low-order linear, time-invariant (LTI) plant models such as those employed in §III.

To obtain a suitable LTI design model, we employ the results of [10] in which system identification experiments were performed to determine low-order LTI climate models for AOGCMs participating in phase 3 of the Coupled Model Intercomparison Project (CMIP3) [11], and whose dynamic behavior is emulated by MAGICC. In the present paper, we use the discrete-time model of order $n = 3$ in [10, Table 2] which very closely reproduces the dynamic behaviour of the default MAGICC climate model with a sampling period of $T_{\mathrm{s}} = 1$ year.

Since the selection of weights in the control design process in §III is more readily performed for continuous-time plant models, the discrete-time climate model is converted to continuous-time form using the bilinear transform $z = \frac{1+sT_{\mathrm{s}}/2}{1-sT_{\mathrm{s}}/2}$, yielding the following design model:

$$G(s) = \frac{0.08517s^3 + 0.2581s^2 + 0.07702s + 0.001456}{s^3 + 1.147s^2 + 0.1687s + 0.002058}. \tag{1}$$

C. Actuators for SRM

Central to the effectiveness of SRM is the ability to appreciably decrease the net flux of solar radiation coming into Earth. This can be achieved either by increasing the planetary albedo (reflectivity) or by physically shading the Earth.

At the top of Earth's atmosphere, the average rate at which solar radiation is received is $342\ \mathrm{Wm}^{-2}$ [12, p. 6]. The average albedo of the Earth is around 30%, resulting in $107\ \mathrm{Wm}^{-2}$ being reflected back to space. The remaining $342-107 = 235\ \mathrm{Wm}^{-2}$ is absorbed, and—assuming thermal equilibrium at the top of the atmosphere—balanced by outgoing longwave (infrared) radiation. Anthropogenic emissions of greenhouse gases into the atmosphere increase the surface temperature at which radiative balance is established, an outcome known as the enhanced greenhouse effect.

Doubling atmospheric CO_2 concentrations from pre-industrial levels would result in a radiative forcing imbalance of approximately $+3.71\ \mathrm{Wm}^{-2}$, a figure which serves as a

useful benchmark against which the effectiveness of various SRM options can be assessed.

Table I lists a number of SRM options reported in [1], together with their associated radiative forcing. Negative forcing denotes an effect counter to the positive imbalance caused by emissions of anthropogenic GHGs. Also included in Table I are the resources needed to achieve the specified radiative forcing. For the most part the defining characteristic of the resource is surface area of land or clouds, though for stratospheric aerosols a more natural metric is the annual quantity of reflective sulphate particles required, listed in Table I in units of teragrams of sulphur per year (TgS yr^{-1}, where $1\ \mathrm{Tg} = 10^{12}\mathrm{g} = 1$ megatonne, Mt).

SRM option	Area (m^2) or other resource	Radiative forcing (Wm^{-2})
Stratospheric aerosols*	1.5–5.0 TgS yr^{-1}	-4.23
Sunshades in space*	4.7×10^{12} at L1	-4.23
Increase marine cloud albedo		
Mechanical*	8.9×10^{13}	-3.71
Biological	5.1×10^{13}	-0.019
Increase land surface albedo		
Desert	1.0×10^{13}	-2.12
Grassland	3.85×10^{13}	-0.51
Cropland	1.4×10^{13}	-0.35
Settlements	3.25×10^{12}	-0.15
Urban areas	1.5×10^{12}	-0.047

TABLE I

RADIATIVE FORCING POTENTIAL OF SRM OPTIONS [1]

For the three options in Table I identified with a superscript *, the indicated area (or other resource) is that required to counteract the radiative forcing due to doubling of atmospheric CO_2. For the remaining options in Table I the radiative forcing corresponds to the estimated maximum potential radiative forcing; see [1] and the references therein for details. (Note that for stratospheric aerosols and space-based sunshades, a radiative forcing of $-4.23\ \mathrm{Wm}^{-2}$ is needed to counter doubled CO_2, as explained in [1, pp. 5546–5547]).

Among the SRM options listed in Table I, injection of reflective stratospheric aerosols [13], [3], [14] and marine cloud brightening [4] are generally regarded as the most plausible on account of their likely technical feasibility and effectiveness at inducing controllable negative radiative forcing. Nevertheless any adoption of SRM would likely involve a portfolio of options, each with its own spatio-temporal effectiveness and risk profile. Modeling the influence of SRM on the climate system as a single actuator as in Fig. 1 clearly obscures a myriad practical details, but nonetheless serves as a useful starting point for the feedback analysis in the sequel.

Table I broadly quantifies the radiative forcing potential of a range of SRM actuator options. To put these figures into context, the radiative forcing imbalance at the present time due to anthropogenic GHGs is increasing at around $+0.057\ \mathrm{Wm}^{-2}\ \mathrm{yr}^{-1}$, having risen by $+0.74\ \mathrm{Wm}^{-2}$ over the period 1990–2013 [15]. This observation raises the closely related issue of the *rate* at which SRM options could reasonably be expected to be deployed, in the event that a decision were made to do so. In a control-theoretic sense, practical constraints on SRM deployment speed impose tight slew-rate constraints on the control output u in Fig. 1.

D. Sensing global temperature

In contrast to the challenges posed by exerting influence over the global climate system via SRM, the task of obtaining measurements of global-mean surface temperature is comparatively straightforward. The most widely used global temperature datasets are those of the Hadley Centre and the Climatic Research Unit (HadCRUT) [16], the NASA Goddard Institute for Space Studies Surface Temperature Analysis (GISTEMP) [17], and the National Climatic Data Center (NCDC) [18]. Inclusion of the term n in Fig. 1 reflects the inevitability of noise in any measurement of global-mean surface temperature.

Extending the time window over which any averaging of temperature is performed can have profound consequences for the design of the SRM feedback controller in Fig. 1. Specifically: averaging introduces delay into the open-loop transfer function KG, reducing gain and phase margins, and raising the prospect of the SRM controller inducing undesirable climatic oscillations; see e.g. [5]. Moreover, natural climate variability on interannual timescales (e.g. El Niño–Southern Oscillation (ENSO)) necessitates the use of extended timescales to smooth short-term trends. The World Meteorological Organization (WMO), for example, uses climate anomalies with respect to 30-year baselines, indicative of the time windows needed to discern long-term climate trends from natural variability.

Time delays associated with averaging of global temperature anomalies over extended windows are in conflict with the stability requirements of discrete-time SRM controllers implemented with (say) 1–5-year sampling periods [5]. The approach taken in this paper is therefore to assume that global temperature measurements are available instantaneously, albeit subject to measurement noise n and natural climate variability. This assumption is consistent with the ready availability of monthly temperature measurements and the use of a sampling period of $T_\mathrm{s} = 1$ year.

E. Disturbances

In addition to the anthropogenic radiative forcing term $\widetilde{R}$ in Fig. 1, the climate system is subject to both solar and volcanic forcing, denoted S and V, respectively. The solar forcing for the period 1880–2010 varies closely with the approximately 11-year solar cycle with a peak–peak magnitude of somewhat less than $0.2\ \mathrm{Wm}^{-2}$, and with negligible trend over the past 50 years [19]./

Volcanic forcing arises from the injection of reflective sulphate particles into the upper atmosphere, with the strength of the forcing being strongly dependent on the occurrence of distinct volcanic events. The short-term cooling effect in the aftermath of major volcanic eruptions is well documented. The 1991 Mount Pinatubo eruption, for example,

is estimated to have caused a global-mean peak forcing of around $-3\ \mathrm{Wm}^{-2}$ [20], leading to a global cooling effect of 0.1–0.3 °C for several years [21]. The cooling influence of volcanic eruptions serves as an obvious naturally-occurring analogue for SRM proposals based on stratospheric aerosol injection.

F. Control objectives

The overarching objective of the SRM controller K in Fig. 1 is to generate a negative radiative forcing term u to offset some of the anthropogenic forcing $\widetilde{R}$ which drives warming of the climate system G. While the extent of the offset is governed by the setpoint (reference) temperature T_{ref}, the control design objective is principally viewed in this paper as a disturbance regulation problem. That is: the controller K should be designed to counter the influence of (some fraction of) anthropogenic forcing $\widetilde{R}$, without unduly amplifying the influence of solar and volcanic disturbances (S and V, resp.), or measurement noise n.

The use of feedback mitigates against uncertainty in the climate model G and the influence of climate feedbacks (dashed line in Fig. 1) on the gas-cycle.

Most importantly, the closed-loop bandwidth of the resulting SRM control system should be designed with a view to constraining both the magnitude and the rate of change in the control signal u, reflecting the limited control authority and responsiveness of SRM actuators.

III. CONTROLLER DESIGN

In this section we describe an approach to SRM controller design as an application of the well-known H_∞-synthesis technique [22], [23], [24]. This approach formalises SRM as a (sub)-optimal disturbance rejection problem, in keeping with the control objectives outlined in §§II-F.

A. H_∞-synthesis

The SRM feedback system in Fig. 1 can be expressed in the standard control configuration shown in Fig. 2. Here the augmented system $P(s)$ includes not only the plant $G(s)$ but weighting functions $W_i(s), i = 1, 2, 3$ which are used to provide user-selectable trade-offs between competing control design objectives.

In Fig. 2, $w = [w_1\ \ w_2]^T$ is the vector of exogenous signals, $z = [z_1\ z_2]^T$ is the vector of error signals which are to be minimized (in the H_∞-norm sense, to be made precise shortly) in order to meet the control objectives, and y and u are the input and output of the controller, respectively. The correspondences between signals in Figs. 1 and 2 are as follows: $w_1 = T_{\mathrm{ref}}$, $w_2 = \widetilde{R} + S + V$, $z_1 = W_1(T_{\mathrm{ref}} - T)$, $z_2 = W_2 u$ and $y = T_{\mathrm{ref}} - T$. While the signal n in Fig. 1 is omitted from Fig. 2, the influence of measurement noise is nonetheless explicitly incorporated into the controller design problem as explained below.

The standard control system in Fig. 2 is described by

$$\begin{array}{rcl} \left[\begin{array}{c} z \\ y \end{array}\right] & = & P(s)\left[\begin{array}{c} w \\ u \end{array}\right] = \left[\begin{array}{cc} P_{11}(s) & P_{12}(s) \\ P_{21}(s) & P_{22}(s) \end{array}\right]\left[\begin{array}{c} w \\ u \end{array}\right] \\ u & = & K(s)y. \end{array}$$

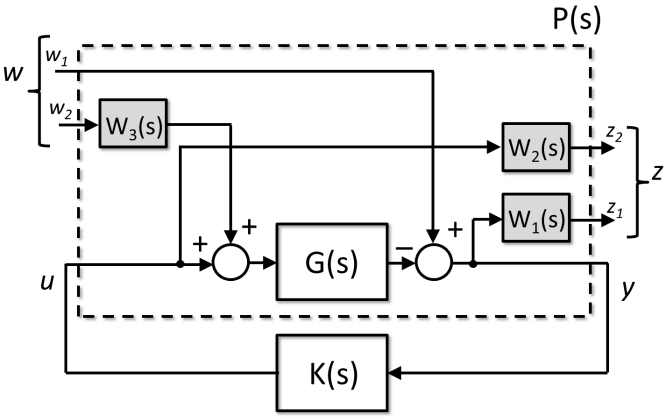

Fig. 2. Augmented system $P(s)$ and SRM controller $K(s)$ in standard control configuration. Exogenous signals consist of the temperature reference w_1 and combined anthropogenic/solar/volcanic forcing w_2, while the error signals are the temperature tracking error z_1 and SRM actuator signal z_2, weighted by $W_1(s)$ and $W_2(s)$, respectively.

The closed-loop transfer function from w to z is given by the linear fractional transformation

$$z = T_{zw}(P, K)w,$$

where

$$T_{zw}(P, K) = P_{11} + P_{12}K(I - P_{22}K)^{-1}P_{21}.$$

The H_∞-optimal control problem finds a stabilizing controller $K(s)$ which minimizes the H_∞-norm of the closed-loop transfer function $T_{zw}(P, K)$, denoted $\|T_{zw}(P, K)\|_\infty := \sup_\omega \bar{\sigma}(T_{zw}(P, K)(j\omega))$, where $\bar{\sigma}(\cdot)$ is the maximum singular value. The motivation for the use of the H_∞-norm in the context of disturbance rejection is its well-known time-domain interpretation as the induced (worst-case) 2-norm:

$$\|T_{zw}(P, K))\|_\infty = \max_{w(t)\neq 0} \frac{\|z(t)\|_2}{\|w(t)\|_2}, \qquad (2)$$

where $\|z(t)\|_2 := \sqrt{\int_0^\infty \Sigma_i |z_i(t)|^2 \mathrm{d}t}$ is the 2-norm of the vector signal z.

While the description above defines the *H_∞-optimal* control problem, in this paper we will be satisfied with solving the computationally simpler *H_∞-suboptimal* control problem, which finds a stabilizing controller $K(s)$ with performance close to optimal as measured by the H_∞-norm. Define $\gamma_{\min}$ as the minimum value of $\|T_{zw}(P, K)\|_\infty$ over all stabilizing controllers K. Then given $\gamma > \gamma_{\min}$, the objective of the H_∞-suboptimal control problem is to find a stabilizing controller $K(s)$ such that $\|T_{zw}(P, K)\|_\infty < \gamma$.

B. Weighting functions

The closed-loop transfer function matrix mapping $[w_1\ w_2]^T$ to $[z_1\ z_2]^T$ is given by

$$T_{zw}(P, K) = \left[\begin{array}{cc} W_1\frac{1}{1+GK} & -W_1W_3\frac{G}{1+GK} \\ W_2\frac{K}{1+GK} & -W_2W_3\frac{GK}{1+GK} \end{array}\right].$$

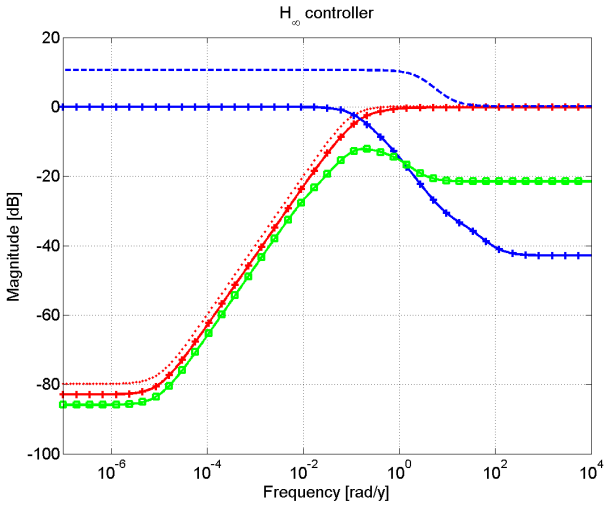

Fig. 3. Sensitivity function (solid, $+$) with upper bound ($\cdots$), and complementary sensitivity function (solid, $\circ$) with upper bound (- -) arising from the controller $K_\infty(s)$ in (5). Disturbance-to-output transfer function $G\mathbf{S}$ shown with $\square$

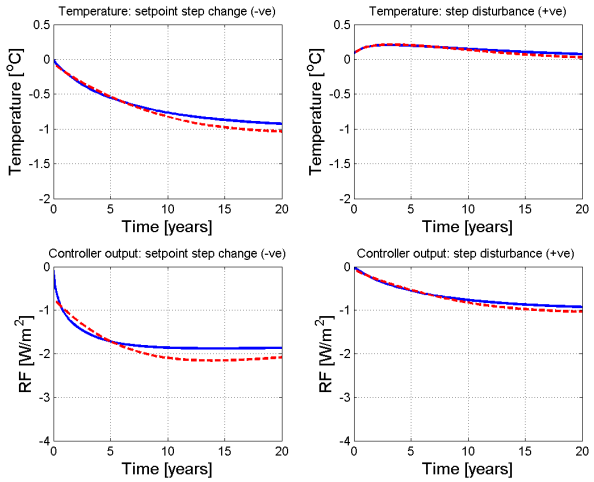

Fig. 4. Time-domain responses for H_∞ and PI controllers. Response of H_∞ controller (—); PI controller (- -)

Since $\|T_{zw}(P,K)\|_\infty < \gamma$ for any H_∞-suboptimal controller:

$$|\mathbf{S}| := \left|\frac{1}{1+GK}\right| \le \frac{\gamma}{|W_1|}, |\mathbf{T}| := \left|\frac{GK}{1+GK}\right| \le \frac{\gamma}{|W_2W_3|} \quad (3)$$

$$\left|\frac{K}{1+GK}\right| \le \frac{\gamma}{|W_2|}, \left|\frac{G}{1+GK}\right| \le \frac{\gamma}{|W_1W_3|}, \quad (4)$$

where the sensitivity ($\mathbf{S}$) and complementary sensitivity ($\mathbf{T}$) functions are defined in (3).

Weighting functions W_1, W_2 and W_3 were tuned as follows to ensure adequate disturbance rejection, reference tracking and closed-loop bandwidth: $W_1(s) = \frac{s+0.1}{s+10^{-5}}, W_2(s) = \frac{s+3}{s+10}, W_3(s) = 1$. The H_∞-suboptimal controller obtained using the `hinfsyn` command in the MATLAB Robust Control Toolbox [25] is as follows:

$$K_\infty(s) = \frac{0.08517s^5+8.9s^4+88.96s^3+85.96s^2+12.11s+0.1591}{s^5+34.46s^4+102.6s^3+36.94s^2+0.8057s+8.053\times10^{-6}}. \quad (5)$$

Fig. 3 shows the sensitivity and complementary sensitivity functions arising from the use of controller (5), along with their frequency-dependent upper bounds. The absence of any pronounced peak in $|\mathbf{T}|$ ensures that measurement noise is not amplified by controller (5). Also shown in Fig. 3 is the transfer function $G\mathbf{S} = G/(1+GK)$, which is the closed-loop transfer function from input disturbance to plant output in Fig. 1. Controller (5) yields $\|G\|_\infty = -12.2$ dB, ensuring effective suppression of input disturbances on T.

C. PI controller

While the H_∞-suboptimal controller (5) was designed using a formal optimization-based framework, the results of MacMartin et al. [5] indicate that a simpler proportional-integral (PI) controller is sufficient to obtain satisfactory performance. In the present paper the following PI controller was obtained via manual tuning:

$$K_{\rm PI}(s) = 0.8 + \frac{0.4}{s}. \quad (6)$$

IV. SIMULATION EXPERIMENTS

A. Simulation with low-order LTI design model

The SRM control system in Fig. 1 was simulated for both the H_∞ controller $K_\infty(s)$ in (5) and the PI controller $K_{\rm PI}(s)$ in (6), using the LTI climate design model $G(s)$ in (1). The temperature response T along with the associated SRM radiative forcing u are shown in Fig. 4, where for each controller the responses to a -1.0 °C change in setpoint temperature $T_{\rm ref}$ and $+1.0$ Wm^{-2} input step disturbance $\widetilde{R}$ were separately simulated. In each simulation experiment the solar and volcanic radiative forcing terms were set to zero.

The responses in Fig. 4 illustrate the speed with which the SRM control system is able to respond to step changes in setpoint and climate disturbances using the controllers in (5) and (6). Any increase in responsiveness is at the expense of increased magnitude or rate of decrease in the required negative radiative forcing.

B. Simulation with real-world proxy model (MAGICC)

The performance of the SRM control system in Fig. 1 was also simulated in discrete-time using the real-world proxy climate model MAGICC. Using the bilinear transform $s = \frac{2}{T_{\rm s}}\frac{z+1}{z-1}$ for sampling period $T_{\rm s} = 1$ year, the continuous-time controllers (5) and (6) were converted to discrete-time:

$$K_\infty(z) = \frac{0.7884z^5-0.4732z^4-1.126z^3+0.6091z^2+0.3669z-0.1623}{z^5-1.598z^4-0.3293z^3+1.368z^2-0.3412z-0.1001}, \quad (7)$$

$$K_{\rm PI}(z) = \frac{z-0.6}{z-1}. \quad (8)$$

The scenario simulated with the real-world proxy model employs SRM from time $t_{\rm SRM} = 2040$ in order to return

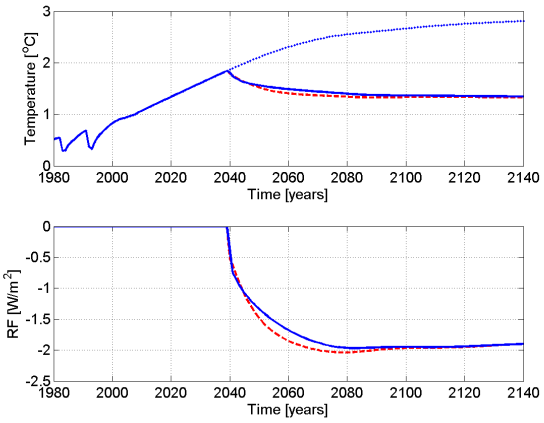

Fig. 5. SRM simulation using MAGICC climate model: H_∞ (—) and PI (- -) controllers. RCP4.5 temperature projection ($\cdots$)

the global-mean surface temperature anomaly to its value in the year 2020 [5]. As a baseline "business as usual" (BAU) case, we use the GHG emissions profile RCP4.5 [26]. Under emissions profile RCP4.5 the best-estimate projected temperature in 2020, and therefore the value of the setpoint $T_{\rm ref}$, is 1.34 °C above its pre-industrial value.

Fig. 5 shows the simulated response of the temperature and SRM forcing signal under the influence of controllers (7) and (8) when the MAGICC default climate model [9] is used as the real-world proxy, and with climate feedbacks on the gas-cycle enabled. Also shown in Fig. 5 is the temperature trajectory under the assumed BAU emissions pathway RCP4.5. Both the discrete-time H_∞ and PI controllers are seen to effectively reduce global-mean surface temperature by some 0.50 °C over the first 100 years of SRM operation following time $t_{\rm SRM}$. Each controller calls for a maximum and sustained negative radiative forcing of magnitude $\sim$2 Wm^{-2}, attained after some 30–40 years of SRM operation. Note also the importance of *bumpless transfer* [27] when switching from "manual" (BAU) to "automatic" (SRM) mode at time $t_{\rm SRM}$.

V. CONCLUSIONS

Geoengineering is cautiously being considered as a technically feasible (if highly controversial) policy response to the threat of anthropogenic climate change. Notwithstanding the raft of ethical, legal and political ramifications of geoengineering, the results of this paper demonstrate that the problem of designing an SRM feedback controller is not intrinsically difficult per se. Practical constraints, however, on the extent, speed and sustainability of SRM deployment options limit the effectiveness of control authority, cautioning against heavy reliance on feedback to counter uncertainty in the dynamic response of the global climate system.

REFERENCES

[1] T. M. Lenton and N. E. Vaughan, "The radiative forcing potential of different climate geoengineering options," *Atmos. Chem. Phys.*, vol. 9, pp. 5539–5561, 2009.

[2] D. Keith, *A Case for Climate Engineering*. Cambridge, MA: MIT Press, 2013.

[3] P. J. Crutzen, "Albedo enhancement by stratospheric sulfur injections: A contribution to resolve a policy dilemma?" *Climatic Change*, vol. 77, no. 3–4, pp. 211–220, August 2006.

[4] J. Latham, K. Bower *et al.*, "Marine cloud brightening," *Phil. Trans. R. Soc. A*, vol. 370, no. 1974, pp. 4217–4262, 13 September 2013.

[5] D. G. MacMartin, B. Kravitz, D. W. Keith, and A. Jarvis, "Dynamics of the coupled human–climate system resulting from closed-loop control of solar geoengineering," *Clim. Dyn.*, vol. 43, no. 1–2, pp. 243–258, July 2014.

[6] A. Jarvis and D. Leedal, "The Geoengineering Model Intercomparison Project (GeoMIP): A control perspective," *Atmos. Sci. Let.*, vol. 13, no. 3, pp. 157–163, July/September 2012.

[7] B. Kravitz, D. G. MacMartin, D. T. Leedal, P. J. Rasch, and A. J. Jarvis, "Explicit feedback and the management of uncertainty in meeting climate objectives with solar geoengineering," *Environ. Res. Lett.*, vol. 9, no. 4, p. 044006 (7pp), April 2014.

[8] D. G. MacMartin, B. Kravitz, and D. W. Keith, "Geoengineering: the World's largest control problem," in *Proc. 2014 American Control Conf.*, Portland, USA, 4–6 June 2014, pp. 2401–2406.

[9] M. Meinshausen, S. C. B. Raper, and T. M. L. Wigley, "Emulating coupled atmosphere-ocean and carbon cycle models with a simpler model, MAGICC6 Part 1: Model description and calibration," *Atmos. Chem. Phys.*, vol. 11, pp. 1417–1456, 2011.

[10] S. R. Weller, B. P. Schulz, and B. M. Ninness, "Identification of linear climate models from the CMIP3 multimodel ensemble," in *Proc. 19th IFAC World Congress*, Cape Town, South Africa, 24–29 August 2014, pp. 10 875–10 881.

[11] G. A. Meehl, C. Covey *et al.*, "The WCRP CMIP3 multimodel dataset," *Bull. Amer. Meteor. Soc.*, vol. 88, no. 9, pp. 1383–1394, September 2007.

[12] G. K. Vallis, *Climate and the Oceans*. Princeton Uni. Press, 2012.

[13] P. J. Rasch, S. Tilmes *et al.*, "An overview of geoengineering of climate using stratospheric sulphate aerosols," *Phil. Trans. R. Soc. A*, vol. 366, no. 182, pp. 4007–4037, 13 November 2008.

[14] T. M. L. Wigley, "A combined mitigation/geoengineering approach to climate stabilization," *Science*, vol. 314, no. 5798, pp. 452–454, 20 October 2006.

[15] NOAA/ESRL, "The NOAA Annual Greenhouse Gas Index (AGGI)," `http://www.esrl.noaa.gov/gmd/aggi/aggi.html`, [Online], accessed 23 May 2014.

[16] C. P. Morice, J. J. Kennedy, N. A. Rayner, and P. D. Jones, "Quantifying uncertainties in global and regional temperature change using an ensemble of observational estimates: The HadCRUT4 data set," *J. Geophys. Res.*, vol. 117, p. D08101 (22pp), 27 April 2012.

[17] J. Hansen, R. Ruedy, M. Sato, and K. Lo, "Global surface temperature change," *Rev. Geophys.*, vol. 48, no. 4, p. RG4004, 2010.

[18] T. M. Smith, R. W. Reynolds, T. C. Peterson, and J. Lawrimore, "Improvements to NOAA's historical merged land–ocean surface temperature analysis (1880–2006)," *J. Climate*, vol. 21, no. 10, pp. 2283–2296, May 2008.

[19] J. L. Lean and D. H. Rind, "How natural and anthropogenic influences alter global and regional surface temperatures: 1889 to 2006," *Geophys. Res. Lett.*, vol. 35, no. 18, p. L18701 (6pp), September 2008.

[20] D. W. J. Thompson, J. M. Wallace, P. D. Jones, and J. J. Kennedy, "Identifying signatures of natural climate variability in time series of global-mean surface temperature: Methodology and insights," *J. Climate*, vol. 22, no. 22, pp. 6120–6141, November 2009.

[21] A. Robock and J. Mao, "The volcanic signal in surface temperature observations," *J. Climate*, vol. 8, no. 5, pp. 1086–1103, May 1995.

[22] J. C. Doyle, K. Glover, P. P. Khargonekar, and B. A. Francis, "State-space solutions to standard $\mathcal{H}_2$ and $\mathcal{H}_\infty$ control problems," *IEEE Trans. Automat. Control*, vol. 34, no. 8, pp. 831–847, August 1989.

[23] K. Zhou, J. C. Doyle, and K. Glover, *Robust and Optimal Control*. Prentice Hall, 2008.

[24] S. Skogestad and I. Postlethwaite, *Multivariable Feedback Control: Analysis and Design*, 2nd ed. Wiley, 2005.

[25] MATLAB, "*Robust Control Toolbox*, version 4.2 (r2012b)," Natick, MA: The MathWorks Inc., 2012.

[26] M. Meinshausen, S. J. Smith *et al.*, "The RCP greenhouse gas concentrations and their extensions from 1765 to 2300," *Climatic Change*, vol. 109, no. 1–2, pp. 213–241, November 2011.

[27] K. J. Åström and B. Wittenmark, *Computer Controlled Systems: Theory and Design*. Englewood Cliffs, NJ: Prentice-Hall, 1984.